ASTRONOMY & ASTROPHYSICS
SUPPLEMENT SERIES

FEBRUARY I **2000**, PAGE 371

Astron. Astrophys. Suppl. Ser. **141**, 371–383 (2000)

Evolutionary tracks and isochrones for low- and intermediate-mass stars: From 0.15 to 7 $M_\odot$, and from $Z = 0.0004$ to 0.03

L. Girardi[1,2,3], **A. Bressan**[4], **G. Bertelli**[1,5], **and C. Chiosi**[1]

[1] Dipartimento di Astronomia, Università di Padova, Vicolo dell'Osservatorio 5, I-35122 Padova, Italy
[2] Max-Planck-Institut für Astrophysik, Karl-Schwarzschild-Str. 1, D-85740 Garching bei München, Germany
[3] Instituto de Física, Universidade Federal do Rio Grande do Sul, Av. Bento Gonçalves 9500, 91501-970 Porto Alegre RS, Brazil
[4] Osservatorio Astronomico di Padova, Vicolo dell'Osservatorio 5, I-35122 Padova, Italy
[5] Consiglio Nazionale delle Ricerche (CNR), Italy

Received June 17; accepted October 29, 1999

Abstract. We present a large grid of stellar evolutionary tracks, which are suitable to modelling star clusters and galaxies by means of population synthesis. The tracks are presented for the initial chemical compositions [$Z = 0.0004, Y = 0.23$], [$Z = 0.001, Y = 0.23$], [$Z = 0.004, Y = 0.24$], [$Z = 0.008, Y = 0.25$], [$Z = 0.019, Y = 0.273$] (solar composition), and [$Z = 0.03, Y = 0.30$]. They are computed with updated opacities and equation of state, and a moderate amount of convective overshoot. The range of initial masses goes from 0.15 $M_\odot$ to 7 $M_\odot$, and the evolutionary phases extend from the zero age main sequence (ZAMS) till either the thermally pulsing AGB regime or carbon ignition. We also present an additional set of models with solar composition, computed using the classical Schwarzschild criterion for convective boundaries. From all these tracks, we derive the theoretical isochrones in the Johnson-Cousins $UBVRIJHK$ broad-band photometric system.

Key words: stars: evolution — stars: interiors — stars: Hertzsprung–Russell (HR) diagram — stars: low-mass

1. Introduction

Models of evolutionary population synthesis require the computation of large data-bases of stellar evolutionary tracks, being as far as possible extended in their interval of initial masses and metallicities, covering the main evolutionary phases, and adopting a homogeneous and updated input physics.

Send offprint requests to: L. Girardi,
e-mail: Lgirardi@pd.astro.it

One of the most popular of these sets is that from the Padova group (Bressan et al. 1993; Fagotto et al. 1994a,b; Bertelli et al. 1994, and references therein). The complete data-base covers a very large range of stellar masses (typically from 0.6 to 120 $M_\odot$) and metallicities (from $Z = 0.0004$ to 0.05). The input physics is homogeneous for all stellar tracks in the grids. Main characteristics of these models are the adoption of OPAL opacities, a constant helium-to-metal enrichment ratio $\Delta Y/\Delta Z$, moderate convective overshooting from convective cores, and mass loss from massive stars. This data-base was extended to very low metallicities (i.e. $Z = 0.0001$) by Girardi et al. (1996a).

Since 1994, many other evolutionary tracks have been computed by us, following some major updatings in the input physics. Some of the new tracks were intended only for testing the effects of these modifications, such as e.g. those discussed in Girardi et al. (1996b). The main novelties with respect to the Bertelli et al. (1994) tracks are, essentially, the adoption of an improved equation of state (Straniero 1988; Girardi et al. 1996a; Mihalas et al. 1990 and references therein), and the new low-temperature opacities from Alexander & Ferguson (1994). Eventually, complete sets of evolutionary tracks have been computed, thus generating a data-base which is comparable to the previous one in terms of the large coverage of mass and metallicity ranges.

This paper aims to present this new data-base of stellar evolutionary tracks and isochrones, and make it available to the users. The tracks presented here are limited to the interval of low- and intermediate mass stars (i.e. from 0.15 to 7 $M_\odot$), and to 6 values of metallicity, from $Z = 0.0004$ to $Z = 0.03$. Further extensions of this data-base will be provided in subsequent papers.

The new evolutionary tracks have already been used in several studies in the last years. They are the starting

point for the detailed thermally pulsing AGB tracks of Marigo (1998a,b) and Marigo et al. (1998, 1999). The stellar chemical yields have been computed by Marigo (1998a) and Marigo et al. (in preparation). An extended sample of the low-mass ZAMS models has been used by Høg et al. (1998) and Pagel & Portinari (1998) in order to access the helium-to-metal enrichment ratio, $\Delta Y/\Delta Z$, for the local stars sampled by the astrometric satellite HIPPARCOS. Girardi (1996) and Girardi & Bertelli (1998) discussed the behaviour of the $B-V$ and $V-K$ integrated colours of single-burst stellar populations derived from the present tracks. Pasquini et al. (in preparation) used the evolution of the momentum of inertia of these models to interpretate observations of disc stars. Girardi et al. (1998) and Girardi (1999) generated synthetic colour-magnitude diagrams (CMD), finding substructures on the clump of red giants of different galaxy models. Finally, the present isochrones were used by Carraro et al. (1999a,b) to derive the ages of the oldest known open clusters.

The plane of this paper is as follows: Sect. 2 presents the input physics of the models; Sect. 3 introduces the stellar tracks and discuss their main characteristics; Sect. 4 describes the mass-loss on the RGB and synthetic TP-AGB evolution; Sect. 5 describes the derived isochrones. Finally Sect. 6 comments on the compatibility of present models with the Bertelli et al. (1994) data-base.

2. Input physics

2.1. Initial chemical composition

Stellar models are assumed to be chemically homogeneous when they settle on the zero age main sequence (ZAMS). The helium and metal mass fractions, Y and Z, are chosen according to some fixed $Y(Z)$ relation. In the present models, the values of $[Z=0.0004, Y=0.23]$, $[Z=0.001, Y=0.23]$, $[Z=0.004, Y=0.24]$, and $[Z=0.008, Y=0.25]$, were chosen in order to coincide with the choices previously adopted in Bertelli et al. (1994, and references therein). On the other hand, the set with solar composition was computed with $[Z=0.019, Y=0.273]$, since this value of Y was fixed by the calibration of the solar model (see Sect. 2.6 below). From these 5 pairs of $[Z,Y]$ values, we obtain an helium-to-metal enrichment relation which is $Y \simeq 0.23 + 2.25\,Z$. We then decide to adopt this mean relation for super-solar metallicities. It gives origin to the values of $[Z=0.03, Y=0.30]$ adopted in our set of highest metallicity.

For each value of Z, the fractions of different metals follow a solar-scaled distribution, as compiled by Grevesse & Noels (1993) and adopted in the OPAL opacity tables. The ratio between abundances of different isotopes is according to Anders & Grevesse (1989).

2.2. Opacities

The radiative opacities are from the OPAL group (Rogers & Iglesias 1992; Iglesias & Rogers 1993) for temperatures higher than $\log(T/\mathrm{K}) = 4.1$, and from Alexander & Ferguson (1994) for $\log(T/\mathrm{K}) < 4.0$. In the temperature interval $4.0 < \log(T/\mathrm{K}) < 4.1$, a linear interpolation between the opacities derived from both sources is adopted. We remind the reader that both opacities sources provide values in good agreement in this temperature interval; the relative differences in opacities are typically lower than 5 percent (see Alexander & Ferguson 1994).

The conductive opacities of electron-degenerate matter are from Hubbard & Lampe (1969). We compared the tracks obtained with this prescription with more recent ones (Salasnich et al., in preparation) which use the Itoh et al. (1983) formulas. No significant differences in the evolutionary features turned out.

2.3. Equation of state

The equation of state (EOS) for temperatures higher than 10^7 K is that of a fully-ionized gas, including electron degeneracy in the way described by Kippenhahn et al. (1965). The effect of Coulomb interactions between the gas particles at high densities is introduced following the prescription by Straniero (1988). The latter was however adapted to the general case of a multiple-component plasma, as described in the Appendix of Girardi et al. (1996a).

For temperatures lower than 10^7 K, we adopt the detailed "MHD" EOS of Mihalas et al. (1990, and references therein). The free-energy minimization technique used to derive thermodynamical quantities and derivatives for any input chemical composition, is described in detail by Hummer & Mihalas (1988), Däppen et al. (1988), and Mihalas et al. (1988). In our cases, we explicitly calculated EOS tables for all the Z values of our tracks, using the Mihalas et al. (1990) code. To save computer time, we consider only the four most abundant metal species, i.e. C, N, O, and Ne. For each Z, EOS tables for several closely spaced values of Y were computed, in order to cover the range of surface helium composition found in the evolutionary models before and after the first and second dredge-up events.

Alternatively, we computed some tracks using a much simpler EOS, where the ionization equilibrium and thermo-dynamical quantities were derived by solving a simple set of Saha equations for a H+He mixture (Baker & Kippenhahn 1962). Comparison of these tracks with those obtained with the MHD EOS revealed that no significant differences in effective temperature or luminosity arise for dwarf stars of mass higher than about 0.7 $M_\odot$, or for giant stars of any mass. This is so because only dwarf stars of lower mass present the dense and

cold envelopes in which the non-ideal effects included in the MHD EOS become important. Moreover, only in the lowest-mass stars the surface temperatures are low enough so that the H_2 molecule is formed, which has dramatic consequences for their internal structures (see e.g. Copeland et al. 1970). Therefore, the use of the MHD EOS is essential for our aim of computing stellar models with masses lower than 0.6 $M_\odot$ (see also Girardi et al. 1996b).

2.4. Reaction rates and neutrino losses

The network of nuclear reactions we use involves all the important reactions of the pp and CNO chains, and the most important alpha-capture reactions for elements as heavy as Mg (see Bressan et al. 1993 and Maeder 1983 for details).

The reaction rates are from the compilation of Caughlan & Fowler (1988), but for $^{17}O(p,\alpha)^{14}N$ and $^{17}O(p,\gamma)^{18}F$, for which we use the more recent determinations by Landré et al. (1990). The uncertain $^{12}C(\alpha,\gamma)^{16}O$ rate was set to 1.7 times the values given by Caughlan & Fowler (1988), as indicated by the study of Weaver & Woosley (1993) on the nucleosynthesis by massive stars. The electron screening factors for all reactions are those from Graboske et al. (1973).

The energy losses by pair, plasma, and bremsstrahlung neutrinos, important in the electron degenerate stellar cores, are taken from Munakata et al. (1985) and Itoh & Kohyama (1983).

2.5. Convection

The energy transport in the outer convection zone is described according to the mixing-length theory of Böhm-Vitense (1958). The mixing length parameter α is calibrated by means of the solar model (see Sect. 2.6 below).

The extension of convective boundaries is estimated by means of an algorithm which takes into account overshooting from the borders of both core and envelope convective zones. The formalism is fully described in Bressan et al. (1981) and Alongi et al. (1991). The main parameter describing overshooting is its extent Λ_c *across* the border of the convective zone, expressed in units of pressure scale heigth. Importantly, this parameter in the Bressan et al. (1981) formalism is not equivalent to others found in literature. For instance, the overshooting scale defined by $\Lambda_c = 0.5$ in the Padova formalism roughly corresponds to the 0.25 pressure scale heigth *above* the convective border, adopted by the Geneva group (Meynet et al. 1994 and references therein) to describe the same physical phenomenum, i.e. $\Lambda_c^G = 0.25$. The non-equivalency of the parameters used to describe convective overshooting by different groups, has been a recurrent source of misunderstanding in the literature.

We adopt the following prescription for the parameter Λ_c as a function of stellar mass:

- Λ_c is set to zero for stellar masses $M \leq 1.0\ M_\odot$, in order to avoid the development of a small central convective zone in the solar model, which would persist up to the present age of 4.6 Gyr;
- For $M \geq 1.5\ M_\odot$, we adopt $\Lambda_c = 0.5$, i.e. a moderate amount of overshoting, which coincides with the values adopted in the previous Bertelli et al. (1994) models;
- In the range $1.0 < M < 1.5\ M_\odot$, we adopt a gradual increase of the overshoot efficiency with mass, i.e. $\Lambda_c = M/M_\odot - 1.0$. This because the calibration of the overshooting efficiency in this mass range is still very uncertain due to the scarcity of stellar data provided by the oldest intermediate-age and old open clusters. Some works (e.g. Aparicio et al. 1990), however, indicate that this efficiency should be lower than in intermediate-mass stars.

In the stages of core helium burning (CHeB), the value $\Lambda_c = 0.5$ is used for all stellar masses. This amount of overshooting dramatically reduces the extent of the breathing pulses of convection found in the late phases of CHeB (see Chiosi et al. 1992).

Overshooting at the lower boundary of convective envelopes is also considered. The calibration of the solar model required an envelope overshooting not higher than 0.25 pressure scale heigths. This value of $\Lambda_e = 0.25$ (see Alongi et al. 1991, for a description of the formalism) was then adopted for the stars with $0.6 \leq (M/M_\odot) < 2.0$, whereas $\Lambda_e = 0$ was adopted for $M < 0.6\ M_\odot$. On the other hand, low values of Λ_e lead to the almost complete suppression of the Cepheid loops in intermediate-mass models (Alongi et al. 1991). Therefore, for $M > 2.5\ M_\odot$ a value of $\Lambda_e = 0.7$ was assumed as in Bertelli et al. (1994). Finally, for masses between 2.0 and 2.5 $M_\odot$, Λ_e was let to increase gradually from 0.25 to 0.7.

We are well aware that the present prescription for the overshooting parameters seems not to fit on the ideals of simplicity and homogeneity one would like to find in such large sets of evolutionary tracks. However, they represent a pragmatic choice, since the prescriptions previously adopted were not satisfactory in many details.

2.6. Calibration of the solar model

The calibration of the solar model is an essential step in the computation of our evolutionary tracks. Some of the parameters found in the solar model are subsequentely adopted in all the stellar models of our data-base.

We adopt for the Sun the metallicity of $Z = 0.019$, i.e. a value almost identical to the $Z_\odot = 0.01886$ favoured by Anders & Grevesse (1989). Several 1 $M_\odot$ models, for different values of mixing-length parameter α and helium content $Y_\odot$, are let to evolve up to the age of 4.6 Gyr. From this series of models, we are able to single out the

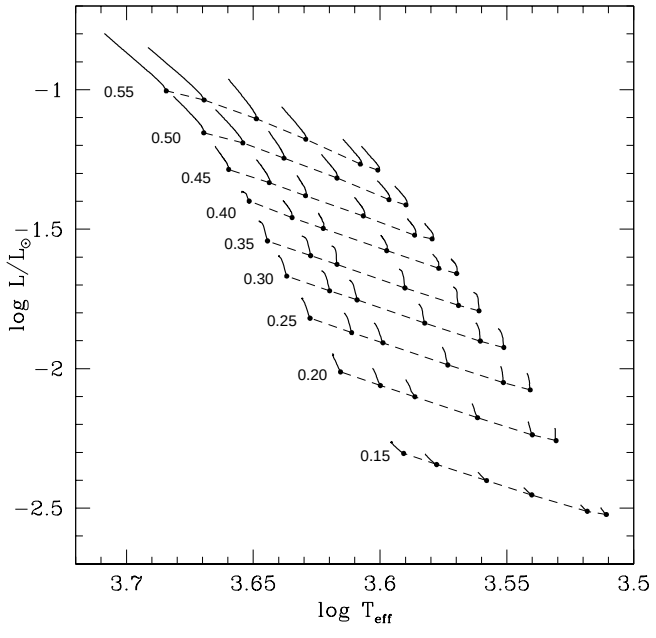

Fig. 1. Evolutionary tracks in the HR diagram, for the models with mass lower than 0.6 $M_\odot$, from the ZAMS up to an age of 25 Gyr. For each star, the evolution starts at the full dot and procedes at increasing luminosity, along the continuous lines. For each stellar mass indicated at the left part of the plot, six tracks are presented, for the metallicity values $Z = 0.0004$, 0.001, 0.004, 0.008, 0.019, 0.030 (along the dashed line, from left to right)

pair of $[\alpha, Y_\odot]$ which allows for a simultaneous match of the present-day solar radius and luminosity, $R_\odot$ and $L_\odot$.

An additional constraint for the solar model comes from the helioseismological determination of the depth of the solar convection zone, of 0.287 ± 0.003 $R_\odot$ (Christensen-Dalsgaard et al. 1991). It corresponds to a radius of $R_c = 0.713$ $R_\odot$ for the lower boundary of the convective envelope. The adoption of an overshooting parameter of $\Lambda_e = 0.7$, like in Bertelli et al. (1994), would lead to a solar model with too a deep convection zone, namely with $R_c = 0.680$ $R_\odot$. This parameter was then reduced to $\Lambda_e = 0.25$, which allows a reasonable reproduction of the observed value of R_c.

Our final solar model reproduces well the Sun $R_\odot$, $L_\odot$, and R_c values. From this model, we derive the values of $\alpha = 1.68$, $Y_\odot = 0.273$, and $\Lambda_e = 0.25$, used in other stellar models as described in the previous subsections.

3. Stellar tracks

3.1. Evolutionary stages and mass ranges

Our models are evolved from the ZAMS, at constant mass. The evolution through the whole H- and He-burning phases is followed in detail. The tracks are stopped either during the TP-AGB phase in intermediate- and low-mass, or at the onset of carbon ignition in a helium-exhausted core in the case of our most massive models. In the case of stellar masses lower than 0.6 $M_\odot$, the main sequence evolution takes place on time scales much larger than a Hubble time. For them, we stopped the computations at an age of about 25 Gyr.

In low-mass stars with $M \gtrsim 0.6$ $M_\odot$, the evolution is interrupted at the stage of He-flash in the electron degenerate hydrogen-exhausted core. This because the computation of the complete evolution through the He-flash requires too much CPU time. The evolution is then restarted from a ZAHB model with the same core mass and surface chemical composition as the last RGB model. The initial ZAHB model presents also a core in which 5 percent (in mass fraction) of the helium has been burned into carbon. This takes into account the approximate amount of nuclear fuel necessary to lift the core degeneracy during the He-flash. The evolution is then followed up to the thermally pulsing AGB phase.

Additional He-burning models with $0.5 \leq (M/M_\odot) < 0.6$ have been computed, starting from a ZAHB model with the same core mass and surface chemical composition as the last 0.6 $M_\odot$ RGB model.

In intermediate-mass stars, the evolution goes from the ZAMS up to either the beginning of the TP-AGB phase, or to the carbon ignition in our most massive models (i.e. those with masses higher than about 5 $M_\odot$).

For the stellar masses in which the evolution goes through the TP-AGB, a small number of thermal pulses has been followed – typically, from 2 to 5 ones. In some few cases, however, the sequences contain only the first significant pulse, whereas few sequences present as much as 19 thermal pulse cycles.

Table 1 gives the values of the transition masses $M_{\rm Hef}$ and $M_{\rm up}$, as derived from the present tracks. $M_{\rm Hef}$ is the maximum mass for a star to develop an electron-degenerate core after the main sequence, and sets the limit between low- and intermediate-mass stars (see e.g. Bertelli et al. 1986; Chiosi et al. 1992). For deriving the values of Table 1, we have selected the stellar track for which the core mass at He-ignition presents its minimum value (see Fig. 1 in Girardi 1999). It coincides, in most cases, with the least massive stellar track we were able to evolve through the He-flash. Given the low mass separation between the tracks we computed, the $M_{\rm Hef}$ values here presented are uncertain by only 0.05 $M_\odot$.

$M_{\rm up}$ is the maximum mass for a star to develop an electron-degenerate core after the CHeB phase, and sets the limit between intermediate- and high-mass stars (Chiosi et al. 1992). Stars with $M > M_{\rm up}$ should ignite carbon and avoid the thermally pulsing AGB phase. Since we do not follow the carbon burning in detail, as soon a small amount of carbon burning occurs in the stars with mass above ~ 4.5 $M_\odot$, we are not able to determine with confidence whether such burning will increase or fade away

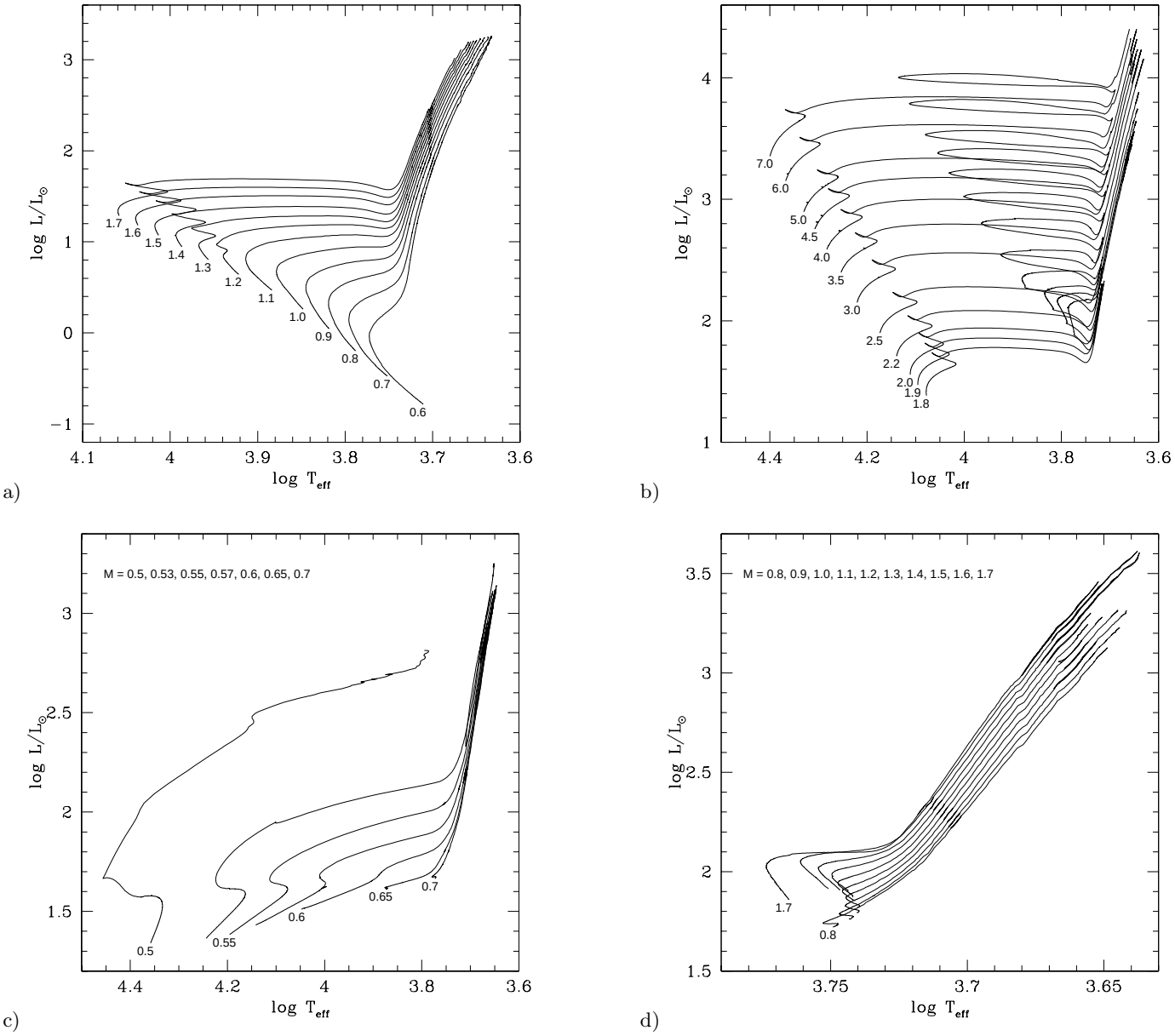

Fig. 2. Evolutionary tracks in the HR diagram, for the composition $[Z = 0.0004, Y = 0.23]$. For most tracks of low-mass stars up to the RGB-tip (panel a), and intermediate-mass ones up to the TP-AGB (panel b), the stellar mass (in $M_\odot$) is indicated at the initial point of the evolution. For the low-mass tracks from the ZAHB up to the TP-AGB (panels c and d), we indicate the complete range of stellar masses in the upper part of the plots

with time (giving place to an AGB star). Therefore, in Table 1 we simply give a range of possible values to $M_{\rm up}$, where the lower limit represents stars which probably enter in the double-shell thermally pulsing phase, and the upper limit that of stars which apparently burn carbon explosively.

3.2. Tracks in the HR diagram

The complete set of tracks for very low-mass stars ($M < 0.6\ M_\odot$) are presented in the HR diagram of Fig. 1.

Table 1. The transition masses $M_{\rm Hef}$ and $M_{\rm up}$

Z	Y	overshoot	$M_{\rm Hef}/M_\odot$	$M_{\rm up}/M_\odot$
0.0004	0.230	moderate	1.7	$4.5 - 5.0$
0.001	0.230	moderate	1.7	$4.5 - 5.0$
0.004	0.240	moderate	1.8	$4.5 - 5.0$
0.008	0.250	moderate	1.9	$4.5 - 5.0$
0.019	0.273	moderate	2.0	$5.0 - 6.0$
0.030	0.300	moderate	2.1	$5.0 - 6.0$
0.019	0.273	no	2.4	$6.0 - 7.0$

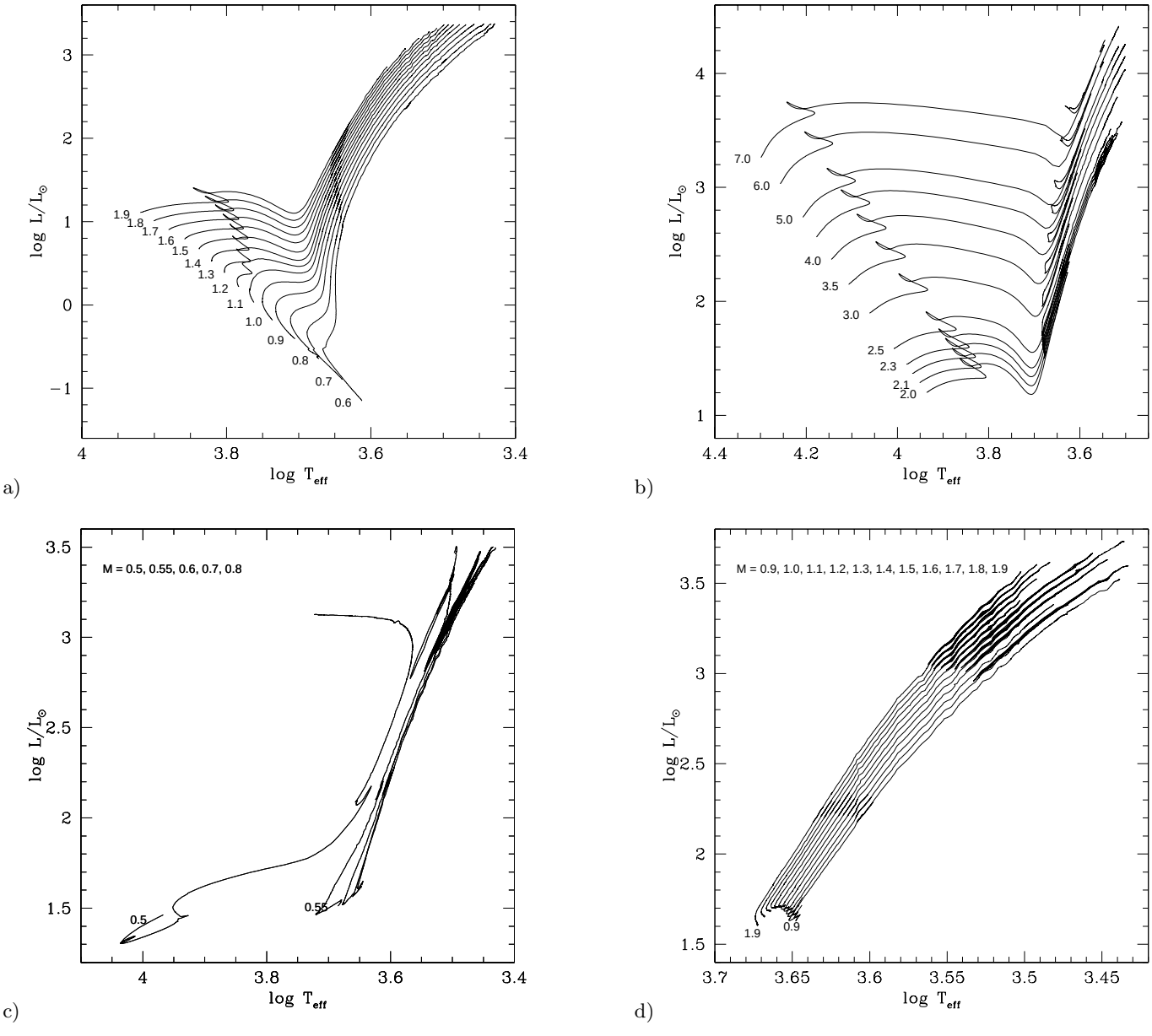

Fig. 3. The same as Fig. 2, but for $[Z = 0.030, Y = 0.300]$

The tracks start at a stage identified with the ZAMS, and end at the age of 25 Gyr. The ZAMS model is defined to be the stage of minimum $T_{\rm eff}$ along the computed track; it follows a stage of much faster evolution in which the pp-cycle is out of equilibrium, and in which gravitation may provide a non negligible fraction of the radiated energy. It is evident from Fig. 1 that these stars evolve very little during the Hubble time.

The complete sets of evolutionary tracks with $[Z = 0.0004, Y = 0.273]$ and $[Z = 0.03, Y = 0.30]$ are presented in the HR diagrams of Figs. 2 and 3, respectively. In these figures, panel (a) presents the low-mass tracks from the ZAMS up to the RGB-tip, panel (b) the intermediate-mass ones from the ZAMS up to the last computed model (either on the TP-AGB phase or during C-ignition, depending on the mass), whereas panels (c) and (d) present the low-mass tracks from the ZAHB up to the TP-AGB phase. Figures 2 and 3 are aimed to illustrate the typical features and mass coverage of the present tracks, at the extreme values of metallicity for which they have been computed. The reader can notice, for instance, the extended Cepheid loops present in the $Z = 0.0004$ intermediate-mass models, which are practically missing in the $Z = 0.03$ ones.

We also computed an additional set of "canonical" evolutionary tracks with solar composition, i.e. $[Z = 0.019, Y = 0.273]$. They differ from the models previously described only in the prescription for the mixing: they are

computed assuming the classical Schwarzschild criterion for the convective boundaries (i.e. without overshooting). Semi-convection is assumed during the core-He burning phase. This set is presented only for $M \geq 1.2\ M_{\odot}$, since stars with $M \lesssim 1.1\ M_{\odot}$ present a radiative core during the main sequence; therefore, the tracks of lower mass are not affected by the adoption of an overshooting scheme (see also Sect. 2.5), at least in the main sequence phase. The two sets of tracks for $[Z = 0.019, Y = 0.273]$ provide a useful data-base for comparing the behaviour of canonical and overshooting models.

3.3. Description of the tables

The data tables for the present evolutionary tracks are available only in electronic format. They are stored at the CDS data center in Strasbourg, and are also available upon request to the authors. A WWW site with the complete data-base (including additional data and the future extensions) will be mantained at http://pleiadi.pd.astro.it

For each evolutionary track, the corresponding data file presents 21 columns with the following information:

1. `age/yr`: stellar age in yr;
2. `logL`: logarithm of surface luminosity (in solar units), $\log(L/L_{\odot})$;
3. `logTef`: logarithm of effective temperature (in K), $\log T_{\rm eff}$;
4. `grav`: logarithm of surface gravity (in cgs units);
5. `logTc`: logarithm of central temperature (in K);
6. `logrho`: logarithm of central density (in cgs units);
7. `Xc,Yc`: mass fraction of either hydrogen (up to the central H-exhaustion) or helium (later stages) in the stellar centre;
8. `Xc_C`: mass fraction of carbon in the stellar centre;
9. `Xc_O`: mass fraction of oxygen in the stellar centre;
10. `Q_conv`: fractionary mass of the convective core;
11. `Q_disc`: fractionary mass of the first mesh point where the chemical composition differs from the surface value;
12. `logL_H`: logarithm of the total luminosity (in solar units) provided by H-burning reactions;
13. `Q1_H`: fractionary mass of the inner border of the H-rich region;
14. `Q2_H`: fractionary mass of the outer border of the H-burning region;
15. `logL_He`: logarithm of the total luminosity (in solar units) provided by He-burning reactions; a null value indicates negligible energy generation by those reactions;
16. `Q1_He`: fractionary mass of the inner border of the He-burning region;
17. `Q2_He`: fractionary mass of the outer border of the He-burning region;
18. `logL_C`: logarithm of the total luminosity (in solar units) provided by C-burning reactions; a null value means that it is negligible;
19. `logL_nu`: logarithm of the total luminosity (in solar units) lost by neutrinos; a null value means that it is negligible;
20. `Q_Tmax`: fractionary mass of the point with the highest temperature inside the star;
21. `stage`: label indicating particular evolutionary stages.

A number of evolutionary stages are indicated along the tracks (Col. 21). They correspond either to: the initial evolutionary stages (`ZAMS` or `ZAHB`), local maxima and minima of L and $T_{\rm eff}$ (`Te-M`, `Te-m`, `L-M`, and `L-m`), the exhaustion of central hydrogen (`Xc=0`) and helium (`Yc=0`), the lowest L and highest $T_{\rm eff}$ during the He-burning of intermediate-mass stars (`Bhe` and `LpT`, respectively), the base and tip of the first ascent of the red giant branch (`Brg` and `Tip`, respectively), the maximum L immediately preceding a thermal pulse (`1tp`), and the onset of C-burning (`Cb`). These stages delimit characteristic evolutionary phases, and can be useful for the derivation of physical quantities (as e.g. typical lifetimes) as a function of either mass or metallicity. Notice that some of these evolutionary stages may be absent from particular tracks, depending on the precise value of stellar mass and metallicity.

For the sake of conciseness and homogeneity, the evolutionary tracks in the data-base do not include the fraction of the TP-AGB evolution which was actually computed, and which is also presented in Figs. 2 and 3. Detailed data about the initial TP-AGB evolution, for any metallicity, can be obtained upon request to the authors. However, we remark that the complete TP-AGB evolution is included, in a synthetic way, in the isochrones to be described below.

3.4. Changes in surface chemical composition

The surface chemical composition of the stellar models change on two well-defined dredge-up events. The first one occurs at the first ascent of the RGB for all stellar models (except for the very-low mass ones which are not evolved out of the main sequence). The second dredge-up is found after the core He-exhaustion, being remarkable only in models with $M \gtrsim 3.5\ M_{\odot}$. We provide tables with the surface chemical composition of H, ^{3}He, ^{4}He, and main CNO isotopes, before and after these events (when present in our data). Table 2 shows, as an example, the table for the solar composition.

4. Mass loss on the RGB, and synthetic TP-AGB evolution

Before presenting the isochrones derived from our evolutionary tracks, we briefly describe the way we have considered the effect of mass loss on the RGB. Also, we describe the extension of our tracks of low- and intermediate-mass stars through the complete TP-AGB phase. The latter

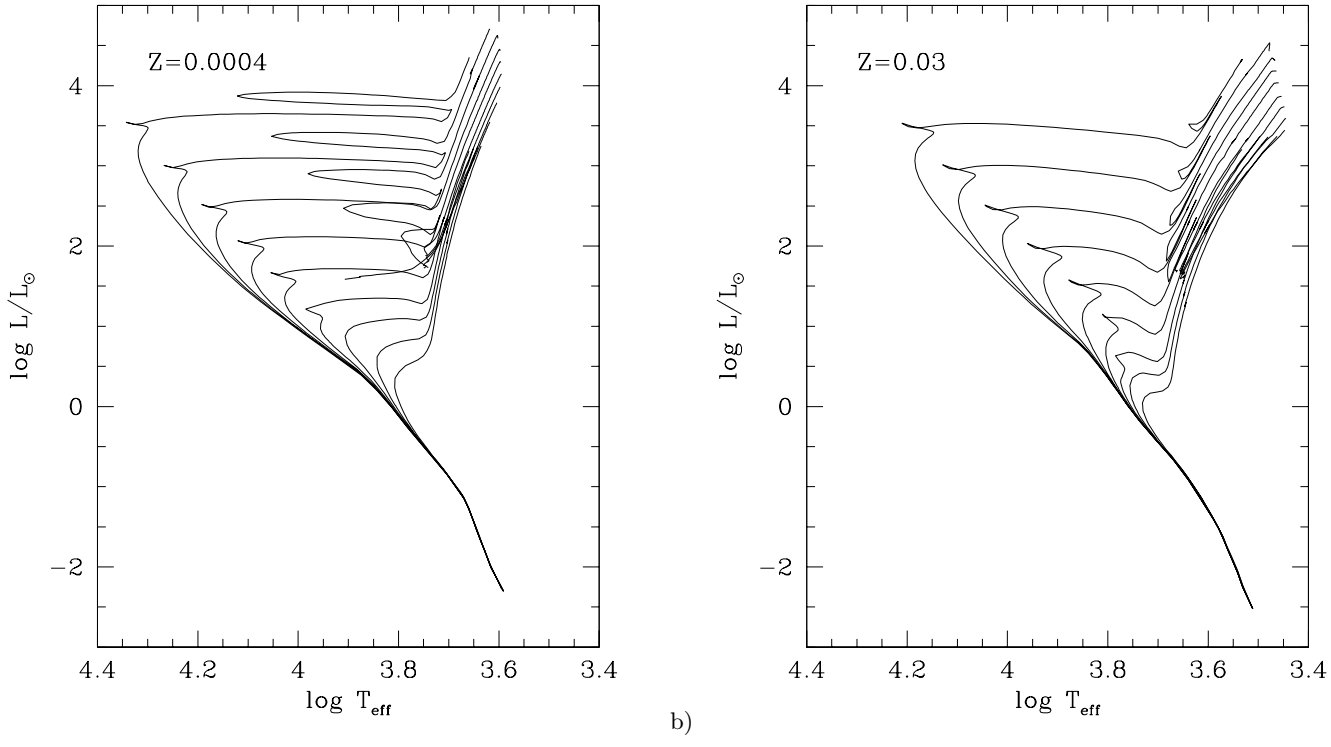

Fig. 5. Theoretical isochrones in the HR diagram, for the compositions $[Z = 0.0004, Y = 0.230]$ (panel a), and $[Z = 0.030, Y = 0.300]$ (panel b). The age range goes from $\log(t/\mathrm{yr}) = 7.8$ to 10.2, at equally spaced intervals of $\Delta \log t = 0.3$. In both cases, the main sequence is complete down to 0.15 $M_\odot$

point is an important one, since this evolutionary phase constitutes a significant fraction of the bolometric luminosity of stellar populations.

Mass loss by stellar winds during the RGB of low-mass stars is considered only at the stage of isochrone construction. We use the empirical formulation by Reimers (1975), but with mass-loss rates multiplied by a parameter η which is set equal to 0.4 (see Renzini & Fusi Pecci 1988). The procedure is basically the following: In passing from the RGB-tip to the ZAHB, we first integrate the mass loss rate along the RGB of every single track, in order to estimate the total amount of mass that has to be removed. Then the mass of the evolutionary models (that were computed at constant mass) is simply scaled down to the value suited to the ZAHB stars. This approximation is a good one since the mass loss does not affect significantly the internal structure of models at the tip of the RGB.

In addition, before constructing the isochrones, we need to complete the stellar evolution along the TP-AGB. This phase is followed in a synthetic way (see Iben & Truran 1978; Groenewegen & de Jong 1993; Bertelli et al. 1994; Marigo et al. 1996, 1998; Girardi & Bertelli 1998). In a few words, we evolve the core mass, total mass, effective temperature and luminosity of each star, from the first thermal pulse on the AGB up to the stage of complete envelope ejection. The following relations are used to this aim:

- The core mass–luminosity relation described in Eqs. (10) and (11) of Groenewegen & de Jong (1993, and references therein);
- The rate of core growth from Eq. (18) of Groenewegen & de Jong (1993);
- The luminosity–effective temperature relations described in Eq. (12) of Girardi & Bertelli (1998). Suffice it to recall that these relations are obtained by extrapolating the slope of the early-AGB phase of our models to higher luminosities and lower effective temperatures. This is performed separately for each value of the metallicity;
- We adopt the Vassiliadis & Wood's (1993) prescription for the mass-loss along the TP-AGB, since it proved to provide a reasonable description for the initial–final relation of low- and intermediate-mass stars of solar metallicity (see e.g. Marigo 1998a), as well as to the maximum luminosity of AGB stars of different ages (and hence initial masses) observed in the LMC (see Marigo et al. 1996).

It is worth remarking that this prescription for the TP-AGB evolution can be considered only as a crude first approximation to the real evolution. We do not consider, for instance, key processes as the third dredge-up and hot-bottom burning in TP-AGB stars. We intend to replace soon the present prescription, for the detailed TP-AGB models of Marigo et al. (1998).

Table 2. Surface chemical composition (by mass fraction) of $[Z = 0.019, Y = 0.273]$ models

$M/M_\odot$	H	^{3}He	^{4}He	^{12}C	^{13}C	^{14}N	^{15}N	^{16}O	^{17}O	^{18}O
Initial:										
all	0.708	$2.92\,10^{-5}$	0.273	$3.26\,10^{-3}$	$3.92\,10^{-5}$	$1.01\,10^{-3}$	$3.97\,10^{-6}$	$9.15\,10^{-3}$	$3.70\,10^{-6}$	$2.06\,10^{-5}$
After the first dredge-up:										
0.60	0.697	$3.03\,10^{-3}$	0.281	$3.25\,10^{-3}$	$4.10\,10^{-5}$	$1.01\,10^{-3}$	$3.93\,10^{-6}$	$9.14\,10^{-3}$	$3.71\,10^{-6}$	$2.06\,10^{-5}$
0.70	0.693	$2.35\,10^{-3}$	0.285	$3.24\,10^{-3}$	$5.62\,10^{-5}$	$1.01\,10^{-3}$	$3.71\,10^{-6}$	$9.15\,10^{-3}$	$3.71\,10^{-6}$	$2.06\,10^{-5}$
0.80	0.691	$1.86\,10^{-3}$	0.288	$3.16\,10^{-3}$	$8.49\,10^{-5}$	$1.07\,10^{-3}$	$3.47\,10^{-6}$	$9.14\,10^{-3}$	$3.71\,10^{-6}$	$2.05\,10^{-5}$
0.90	0.690	$1.54\,10^{-3}$	0.290	$3.04\,10^{-3}$	$9.52\,10^{-5}$	$1.20\,10^{-3}$	$3.27\,10^{-6}$	$9.15\,10^{-3}$	$3.72\,10^{-6}$	$2.03\,10^{-5}$
1.00	0.690	$1.20\,10^{-3}$	0.290	$2.94\,10^{-3}$	$9.89\,10^{-5}$	$1.32\,10^{-3}$	$3.12\,10^{-6}$	$9.15\,10^{-3}$	$3.75\,10^{-6}$	$1.99\,10^{-5}$
1.10	0.690	$9.83\,10^{-4}$	0.290	$2.83\,10^{-3}$	$1.00\,10^{-4}$	$1.44\,10^{-3}$	$2.98\,10^{-6}$	$9.15\,10^{-3}$	$3.89\,10^{-6}$	$1.94\,10^{-5}$
1.20	0.693	$8.32\,10^{-4}$	0.287	$2.77\,10^{-3}$	$1.02\,10^{-4}$	$1.51\,10^{-3}$	$2.89\,10^{-6}$	$9.14\,10^{-3}$	$4.06\,10^{-6}$	$1.91\,10^{-5}$
1.30	0.695	$7.40\,10^{-4}$	0.286	$2.72\,10^{-3}$	$9.63\,10^{-5}$	$1.57\,10^{-3}$	$2.88\,10^{-6}$	$9.14\,10^{-3}$	$4.31\,10^{-6}$	$1.87\,10^{-5}$
1.40	0.695	$6.78\,10^{-4}$	0.286	$2.61\,10^{-3}$	$1.01\,10^{-4}$	$1.70\,10^{-3}$	$2.68\,10^{-6}$	$9.14\,10^{-3}$	$4.86\,10^{-6}$	$1.82\,10^{-5}$
1.50	0.693	$5.92\,10^{-4}$	0.288	$2.39\,10^{-3}$	$1.07\,10^{-4}$	$1.95\,10^{-3}$	$2.38\,10^{-6}$	$9.14\,10^{-3}$	$6.47\,10^{-6}$	$1.72\,10^{-5}$
1.60	0.693	$5.22\,10^{-4}$	0.287	$2.33\,10^{-3}$	$1.06\,10^{-4}$	$2.03\,10^{-3}$	$2.31\,10^{-6}$	$9.12\,10^{-3}$	$2.00\,10^{-5}$	$1.68\,10^{-5}$
1.70	0.693	$4.57\,10^{-4}$	0.288	$2.28\,10^{-3}$	$1.05\,10^{-4}$	$2.12\,10^{-3}$	$2.26\,10^{-6}$	$9.06\,10^{-3}$	$3.80\,10^{-5}$	$1.65\,10^{-5}$
1.80	0.692	$4.08\,10^{-4}$	0.288	$2.29\,10^{-3}$	$1.08\,10^{-4}$	$2.16\,10^{-3}$	$2.24\,10^{-6}$	$9.00\,10^{-3}$	$4.28\,10^{-5}$	$1.64\,10^{-5}$
1.90	0.691	$3.65\,10^{-4}$	0.289	$2.25\,10^{-3}$	$1.07\,10^{-4}$	$2.25\,10^{-3}$	$2.20\,10^{-6}$	$8.93\,10^{-3}$	$5.13\,10^{-5}$	$1.62\,10^{-5}$
1.95	0.691	$3.45\,10^{-4}$	0.290	$2.25\,10^{-3}$	$1.07\,10^{-4}$	$2.28\,10^{-3}$	$2.20\,10^{-6}$	$8.91\,10^{-3}$	$4.50\,10^{-5}$	$1.62\,10^{-5}$
2.00	0.690	$3.25\,10^{-4}$	0.291	$2.22\,10^{-3}$	$1.03\,10^{-4}$	$2.35\,10^{-3}$	$2.19\,10^{-6}$	$8.86\,10^{-3}$	$5.27\,10^{-5}$	$1.61\,10^{-5}$
2.20	0.687	$2.61\,10^{-4}$	0.294	$2.20\,10^{-3}$	$1.06\,10^{-4}$	$2.48\,10^{-3}$	$2.17\,10^{-6}$	$8.74\,10^{-3}$	$5.13\,10^{-5}$	$1.59\,10^{-5}$
2.50	0.683	$2.09\,10^{-4}$	0.298	$2.21\,10^{-3}$	$1.08\,10^{-4}$	$2.62\,10^{-3}$	$2.13\,10^{-6}$	$8.58\,10^{-3}$	$4.93\,10^{-5}$	$1.59\,10^{-5}$
3.00	0.680	$1.46\,10^{-4}$	0.301	$2.19\,10^{-3}$	$1.08\,10^{-4}$	$2.76\,10^{-3}$	$2.09\,10^{-6}$	$8.47\,10^{-3}$	$3.08\,10^{-5}$	$1.58\,10^{-5}$
3.50	0.682	$1.11\,10^{-4}$	0.299	$2.23\,10^{-3}$	$1.08\,10^{-4}$	$2.71\,10^{-3}$	$2.12\,10^{-6}$	$8.48\,10^{-3}$	$2.13\,10^{-5}$	$1.60\,10^{-5}$
4.00	0.682	$9.04\,10^{-5}$	0.299	$2.26\,10^{-3}$	$1.15\,10^{-4}$	$2.67\,10^{-3}$	$2.11\,10^{-6}$	$8.48\,10^{-3}$	$1.49\,10^{-5}$	$1.63\,10^{-5}$
4.50	0.681	$7.52\,10^{-5}$	0.299	$2.27\,10^{-3}$	$1.17\,10^{-4}$	$2.69\,10^{-3}$	$2.10\,10^{-6}$	$8.44\,10^{-3}$	$1.19\,10^{-5}$	$1.64\,10^{-5}$
5.00	0.680	$6.37\,10^{-5}$	0.300	$2.30\,10^{-3}$	$1.16\,10^{-4}$	$2.70\,10^{-3}$	$2.12\,10^{-6}$	$8.39\,10^{-3}$	$1.16\,10^{-5}$	$1.65\,10^{-5}$
6.00	0.681	$4.93\,10^{-5}$	0.300	$2.35\,10^{-3}$	$1.21\,10^{-4}$	$2.66\,10^{-3}$	$2.14\,10^{-6}$	$8.36\,10^{-3}$	$8.92\,10^{-6}$	$1.67\,10^{-5}$
7.00	0.679	$4.03\,10^{-5}$	0.302	$2.33\,10^{-3}$	$1.20\,10^{-4}$	$2.76\,10^{-3}$	$2.13\,10^{-6}$	$8.28\,10^{-3}$	$7.84\,10^{-6}$	$1.66\,10^{-5}$
After the second dredge-up:										
4.50	0.653	$7.06\,10^{-5}$	0.328	$2.14\,10^{-3}$	$1.14\,10^{-4}$	$3.15\,10^{-3}$	$1.98\,10^{-6}$	$8.09\,10^{-3}$	$1.30\,10^{-5}$	$1.55\,10^{-5}$
5.00	0.635	$5.80\,10^{-5}$	0.346	$2.11\,10^{-3}$	$1.13\,10^{-4}$	$3.42\,10^{-3}$	$1.94\,10^{-6}$	$7.82\,10^{-3}$	$1.23\,10^{-5}$	$1.51\,10^{-5}$
6.00	0.610	$4.29\,10^{-5}$	0.371	$2.07\,10^{-3}$	$1.16\,10^{-4}$	$3.74\,10^{-3}$	$1.89\,10^{-6}$	$7.51\,10^{-3}$	$9.47\,10^{-6}$	$1.49\,10^{-5}$
7.00	0.622	$3.56\,10^{-5}$	0.359	$2.09\,10^{-3}$	$1.16\,10^{-4}$	$3.65\,10^{-3}$	$1.90\,10^{-6}$	$7.58\,10^{-3}$	$8.57\,10^{-6}$	$1.48\,10^{-5}$

For the moment, we just compare the initial–final mass relation, as derived from the present tracks, with the empirical one of Herwig (1996). This is done in Fig. 4. It is important to recall some aspects of the empirical relation. First, the Herwig (1996) relation is very different from the (largely used) Weidemann (1987) one, at least in the range of initial masses $M \gtrsim 2\ M_\odot$; this is due, essentially, to the dramatic re-evaluation of the mass of the white dwarfs in the Hyades (cf. Weidemann 1996). Second, the Herwig (1996) relation extends up to a initial mass of $8\ M_\odot$, value which represents the white dwarfs in the open cluster NGC 2516. Recently, the initial mass of the white dwarfs in this cluster have been re-evaluated, to new values of $5{-}6\ M_\odot$, by Jeffries (1997). Therefore, the upper mass limit of stars which produce white dwarfs, is roughly consistent with the values of $M_{\rm up} \sim 5\ M_\odot$ we find in our stellar models.

Figure 4 evidences that our theoretical initial–final mass relation for the solar metallicity, reproduces in a satisfactory way the empirical one from Herwig (1996) and Jeffries (1997). This is an important point for a set of isochrones aimed to be used in evolutionary population synthesis calculations.

5. Isochrones

5.1. Construction of isochrones

From the tracks presented in this paper, we have constructed isochrones adopting the same algorithm of "equivalent evolutionary points" as used in Bertelli et al. (1990, 1994).

The initial point of each isochrone is the $0.15\ M_\odot$ model in the lower main sequence. The terminal stage of the isochrones is either the tip of the TP-AGB for

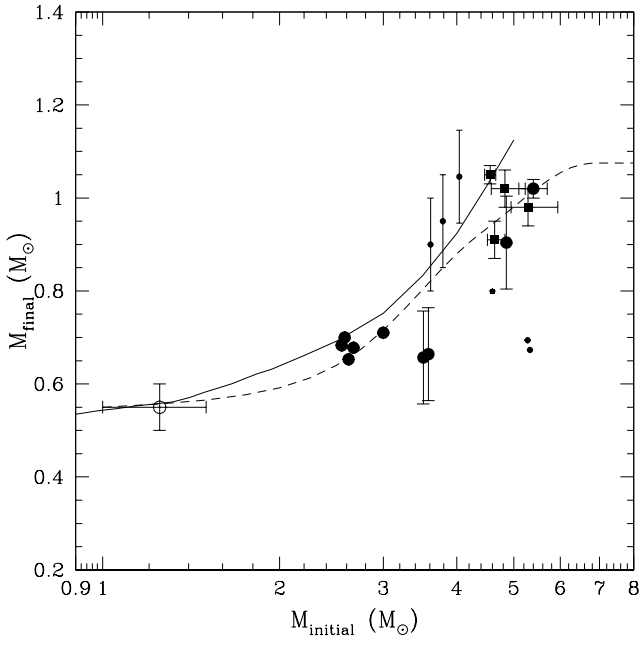

Fig. 4. Comparison between the empirical and theoretical initial–final mass relations. The dots are data for WDs in open clusters, according to Herwig (1996; full circles) and Jeffries (1997, full squares). The smaller dots represent data points of lower quality (cf. Herwig 1996). The open circle instead represents the mean masses of field white dwarfs and their progenitors. The mean initial–final mass relation from Herwig is also shown (dashed line); it is based only in the most reliable mass determinations for white dwarfs. The continuous line, instead, is the initial–final mass relation as derived from our $Z = 0.019$ models (see text for details)

$M \lesssim 5\ M_\odot$ (ages of $\sim 10^8$ yr), or C-ignition in the core for the remaining stars.

Theoretical luminosities and effective temperatures along the isochrones are translated to magnitudes and colors using extensive tabulations of bolometric corrections and colors, as in Bertelli et al. (1994). The tabulations were obtained from convolving the spectral energy distributions contained in the library of stellar spectra of Kurucz (1992) with the response function of several broad-band filters. The response functions are from Buser & Kurucz (1978) for the UBV pass-bands, from Bessell (1990) for the R and I Cousins, and finally from Bessell & Brett (1988) for the JHK ones.

5.2. Description of isochrone tables

In Fig. 5 we present some of the derived isochrones on the HRD, sampled at age intervals of $\Delta \log t = 0.3$. They cover the complete age range from about 0.06 to 16 Gyr. Younger isochrones could be constructed only with the aid of evolutionary tracks for stars with initial masses $M \gtrsim 7\ M_\odot$, which are not presented in this paper.

Complete tables with the isochrones can be obtained at the CDS in Strasbourg, or upon request to the authors, or through the WWW site http://pleiadi.pd.astro.it. In this data-base, isochrones are provided at $\Delta \log t = 0.05$ intervals; this means that any two consecutive isochrones differ by only 12 percent in their ages.

For each isochrone table, the layout is as follows: A header presents the basic information about the age and metallicity of each isochrone. Column 1 presents the logarithm of the age in yr; Cols. 2 and 3 the initial and actual stellar masses, respectively. We recall that the initial mass is the useful quantity for population synthesis calculations, since together with the initial mass function it determines the relative number of stars in different sections of the isochrones. Then follow the logarithms of surface luminosity (Col. 4), effective temperature (Col. 5), and surface gravity (Col. 6). From Cols. 7 to 15, we have the sequence of absolute magnitudes, starting with the bolometric one and following those in the $UBVRIJHK$ pass-bands. In the last Col. (16), the indefinite integral over the initial mass M of the initial mass function (IMF) by number, i.e.

$$\text{FLUM} = \int \phi(M) \mathrm{d}M \qquad (1)$$

is presented, for the case of the Salpeter IMF, $\phi(M) = AM^{-\alpha}$, with $\alpha = 2.35$. When we assume a normalization constant of $A = 1$, FLUM is simply given by $\text{FLUM} = M^{1-\alpha}/(1-\alpha)$. This is a useful quantity since the difference between any two values of FLUM is proportional to the number of stars located in the corresponding mass interval. It is worth remarking that we present FLUM values for the complete mass interval down to 0.15 $M_\odot$, always assuming a Salpeter IMF, whereas we know that such an IMF cannot be extended to such low values of the mass. However, the reader can easily derive FLUM relations for alternative choices of the IMF, by using the values of the initial mass we present in the Col. 2 of the isochrone tables.

We also provide summary tables containing basic information for the most significant stages along the isochrones. A sample table of this kind is presented in Table 3 below, for three $Z = 0.019$ isochrones, with age values log(age/yr) = 7.8, 9.0 and 10.2. The evolutionary stages are listed in the last column, and are, in sequence:

- `TO`: the turn-off point, i.e. the point of highest $T_{\rm eff}$ during the core−H burning phase;
- If present, `Te-m` and `Te-M` signal the coldest and hottest points, respectively, of stars in the overall contraction phase at the end of core−H burning; in this case `Te-M` roughly corresponds to the stars in the stage of core H−exhaustion. Occasionally, this stage is followed by a local maximum of luminosity, `L-M`, of stars which are crossing Hertzsprung gap;
- `RGBb`: the base of the RGB;
- if present, `L-M` and `L-m` limit the luminosity interval of RGB stars which are crossing the discontinuity in

Table 3. Sample summary table with the most significant stages along some $Z = 0.019$ isochrones

log(age/yr)	$M_{\rm ini}$	$M_{\rm act}$	$\log(L/L_\odot)$	$\log T_{\rm eff}$	$\log G$	M_V	$U-B$	$B-V$	$V-I$	stage
7.80	5.6503	5.644	3.147	4.206	3.81	−1.725	−0.643	−0.174	−0.161	TO
7.80	6.3176	6.305	3.474	4.164	3.37	−2.789	−0.586	−0.156	−0.135	Te-m
7.80	6.3592	6.346	3.572	4.223	3.51	−2.690	−0.688	−0.187	−0.167	Te-M
7.80	6.3625	6.349	3.576	4.067	2.88	−3.584	−0.394	−0.113	−0.068	L-M
7.80	6.3666	6.353	3.314	3.656	1.50	−3.026	1.170	1.222	1.155	RGBb
7.80	6.3733	6.356	3.898	3.588	0.64	−3.845	1.806	1.542	1.657	RGBt
7.80	6.4397	6.397	3.491	3.635	1.24	−3.291	1.458	1.348	1.282	BHeb
7.80	6.4899	6.440	3.686	3.819	1.78	−4.523	0.230	0.363	0.431	Te-M
7.80	6.6046	6.530	3.703	3.612	0.94	−3.599	1.697	1.473	1.438	EHeb
7.80	6.6152	6.526	4.317	3.553	0.09	−4.262	1.813	1.581	2.230	Cb
⋮	⋮	⋮	⋮	⋮	⋮	⋮	⋮	⋮	⋮	⋮
9.00	1.7933	1.791	1.160	3.871	3.96	1.826	0.025	0.270	0.308	TO
9.00	2.0510	2.047	1.443	3.825	3.55	1.148	0.004	0.414	0.495	Te-m
9.00	2.0663	2.062	1.609	3.890	3.65	0.693	0.107	0.181	0.205	Te-M
9.00	2.0671	2.063	1.560	3.827	3.45	0.851	0.014	0.406	0.486	L-M
9.00	2.0728	2.068	1.292	3.713	3.26	1.747	0.494	0.883	0.906	RGBb
9.00	2.0866	2.080	2.353	3.635	1.89	−0.454	1.293	1.283	1.280	RGBt
9.00	2.0913	2.084	1.528	3.691	2.94	1.253	0.683	0.991	0.996	BHeb
9.00	2.1686	2.159	1.620	3.692	2.87	1.016	0.677	0.987	0.989	Te-M
9.00	2.2986	2.283	2.113	3.664	2.28	−0.056	0.978	1.135	1.124	EHeb
9.00	2.3080	2.279	3.326	3.564	0.67	−2.051	1.818	1.570	2.000	1TP
9.00	2.3096	0.672	4.069	3.473	−0.97	−1.287	1.377	1.617	3.764	AGBt
⋮	⋮	⋮	⋮	⋮	⋮	⋮	⋮	⋮	⋮	⋮
10.20	0.8938	0.892	0.090	3.742	4.21	4.665	0.269	0.748	0.791	TO
10.20	0.9190	0.917	0.240	3.702	3.91	4.436	0.557	0.917	0.955	RGBb
10.20	0.9321	0.927	1.350	3.653	2.61	1.928	1.021	1.162	1.184	L-M
10.20	0.9324	0.926	1.289	3.656	2.69	2.057	0.984	1.143	1.167	L-m
10.20	0.9342	0.743	3.370	3.485	−0.18	0.191	1.399	1.615	3.577	RGBt
10.20	0.9342	0.743	1.574	3.666	2.35	1.276	0.948	1.121	1.112	BHeb
10.20	0.9343	0.742	1.625	3.661	2.27	1.180	0.999	1.146	1.135	Te-m
10.20	0.9354	0.738	1.586	3.670	2.35	1.220	0.916	1.104	1.093	Te-M
10.20	0.9363	0.735	2.019	3.631	1.76	0.415	1.360	1.311	1.303	EHeb
10.20	0.9363	0.734	2.267	3.609	1.42	0.017	1.647	1.450	1.454	L-M
10.20	0.9363	0.733	2.142	3.620	1.59	0.210	1.502	1.377	1.373	L-m
10.20	0.9365	0.674	3.314	3.487	−0.15	0.275	1.404	1.614	3.537	1TP
10.20	0.9365	0.529	3.499	3.465	−0.53	0.315	1.362	1.618	3.886	AGBt

chemical profile left by the first dredge−up event; so, this interval corresponds to the bump in the luminosity function along the RGB;
- `RGBt`: the tip of the RGB;
- `BHeb`: the beginning of the CHeB phase. It is defined as the point of lowest luminosity for CHeB stars;
- If present, `Te-m` and `Te-M` signal the coldest and hottest points, respectively, for CHeB stars. For the youngest isochrones, `Te-M` represents the maximum extension of the Cepheid loop;
- `EHeb`: the end of the CHeB phase;
- In the oldest isochrones, `L-M` and `L-m` limit the luminosity range of early-AGB stars; this interval corresponds to the clump of early-AGB stars in colour-magnitude diagrams;
- `1TP`: the beginning of the thermally pulsing AGB phase;
- `AGBt`: the end of the AGB phase;
- `Cb`: the stage of C-ignition in the cases the AGB phase does not occur.

Similar tables are presented in the data-base, for other values of age and metallicity.

In addition, we provide tables with the integrated broad-band colours of single-burst stellar populations. Such tables are derived by integrating the stellar luminosities, weighted by the predicted number of stars in each bin, along the isochrones.

6. Concluding remarks

The stellar evolutionary tracks described here constitute a very extensive and homogeneous grid. They are therefore suited to the purposes of evolutionary population synthesis, either of simple (star clusters) or complex (galaxies) stellar populations. They can be used to describe populations older than 6 10^7 yr, for a wide range of metallicities. This range does not include, however, that of very low-metallicities found in some globular clusters, and the tail of very high metallicities which may be found in the most massive elliptical galaxies and bulges. We intend to extend the data-base in order to cover these intervals in forthcoming papers.

One of the main characteristic of this data-base is that stellar tracks are presented at very small mass intervals. The typical mass resolution for low-mass stars is of 0.1 $M_\odot$. This is reduced to 0.05 $M_\odot$ in the interval of very-low masses ($M \lesssim 0.6\ M_\odot$), and occasionally in the vicinity of the limit mass $M_{\rm Hef}$ between low- and intermediate mass stars. The mass separation between tracks increases in the range of intermediate-mass stars, but anyway we provide enough tracks to allow a very detailed mapping of the HR diagram. As a result of this good mass resolution, the derived theoretical isochrones are also very detailed.

Due to their characteristics, the data-base is particularly suited to the construction of synthetic colour-magnitude diagrams (CMD). The latter are important tools for the correct interpretation of the high-quality photometric data which is becoming available for Local Group galaxies. Among these data, we mention the HIPPARCOS results for the solar vicinity (Perryman et al. 1995), the extensive photometric data-bases derived from the search of micro-lensing events towards the Magellanic Clouds and the Galactic Bulge, and deep HST images of particular galaxy fields.

As examples of the level of detail provided by the present tracks and isochrones, we mention the results obtained in the works by Girardi et al. (1998) and Girardi (1999). They have simulated synthetic CMDs for different model galaxies, finding substructures in the red clump region of the CMD. In particular, a faint secondary clump happens to be present in such models, as a result of the fine mass resolution adopted in the calculation of the evolutionary tracks with mass $M \sim 2\ M_\odot$. Counterparts to these clump substructures have been noticed in the CMDs derived from HIPPARCOS data, and those of some Magellanic Cloud fields observed to date (see Girardi 1999).

In addition, the present tracks behave in a very regular way for different metallicities, so that the construction of isochrones for any intermediate value of metallicity (in the interval $0.0004 \leq Z \leq 0.03$) is possible. These isochrones for arbitrary values of Z are available upon request, but are not included in the present electronic data-base.

An open question is whether the present models can be complemented with those of Bertelli et al. (1994) and Girardi et al. (1996a), for metallicities lower than $Z = 0.0004$ and higher than $Z = 0.03$, or masses higher than 7 $M_\odot$. The answer is not simple. In fact there are several differences between both sets of models. First of all, for metallicities higher than $Z = 0.008$, the adopted $Y(Z)$ relations are different. It generates systematic, although small, differences in the model luminosities and lifetimes for the sets of highest metallicities. Whether they are significant, however, is something that depends on the level of detail one is interested to look at.

The Bertelli et al. (1994) data-base does not contain $Z = 0.001$ models with OPAL opacities, which are included in the present one. With respect to lower metallicities, the Girardi et al. (1996a) models with $Z = 0.0001$, are probably a valid complement to the present ones, but present a lower mass resolution than now adopted, and a different prescription for overshooting in the mass range $1.0 < (M/M_\odot) < 1.5$.

On the other hand, a preliminary comparison between the present and previous Padova evolutionary models, in the range from about 5 to 7 $M_\odot$, reveals that they have almost identical tracks in the HRD and lifetimes. Therefore, they can be used to complement the present models for masses higher than 7 $M_\odot$, or equivalently for ages younger than 10^8 yr.

Acknowledgements. We thank D. Mihalas and R. Wehrse for kindly providing us with the "MHD" code for the equation of state, and E. Bica, P. Marigo, B. Salasnich and A. Weiss for the many useful discussions. L. Girardi acknowledges the many people who, in the last years, either lent him computers and CPU time in order to make preliminary calculations to the present tracks (especially M.V.F. Copetti, A.A. Schmidt, S.O. Kepler), or helped in the solution of daily computer problems (especially A. Weiss and B. Salasnich). The work by L. Girardi has been initially funded by the CNPq Brazilian agency, and later by the German Alexander von Humboldt-Stiftung. This work was completed with funding by the Italian MURST.

References

Alexander D.R., Ferguson J.W., 1994, ApJ 437, 879
Alongi M., Bertelli G., Bressan A., Chiosi C., 1991, A&A 244, 95
Anders E., Grevesse N., 1989, Geochim. Cosmochim. Acta 53, 197
Aparicio A., Bertelli G., Chiosi C., Garcia-Pelayo J.M., 1990, A&A 240, 262
Baker N., Kippenhahn R., 1962, Z. Astroph. 54, 114
Bertelli G., Bressan A., Chiosi C., Angerer K., 1986, A&AS 66, 191
Bertelli G., Betto R., Bressan A., et al., 1990, A&AS 85, 845
Bertelli G., Bressan A., Chiosi C., Fagotto F, Nasi E., 1994, A&AS 106, 275
Bessell M.S., 1990, PASP 102, 1181
Bessell M.S., Brett J.M., 1988, PASP 100, 1134

Böhm-Vitense E., 1958, Z. Astroph. 46, 108
Bressan A., Bertelli G., Chiosi C., 1981, A&A 102, 25
Bressan A., Fagotto F., Bertelli G., Chiosi C., 1993, A&AS 100, 647
Buser R., Kurucz R.L., 1978, A&A 70, 555
Carraro G., Vallenari A., Girardi L., Richichi A., 1999a, A&A 343, 825
Carraro G., Girardi L., Chiosi C., 1999b, MNRAS 309, 430
Caughlan G.R., Fowler W.A., 1988, Atomic Data and Nuclear Data Tab. 40, 283
Chiosi C., Bertelli G., Bressan A., 1992, ARA&A 30, 305
Christensen-Dalsgaard J., Gough D.O., Thompson M.J., 1991, A&A 264, 518
Copeland H., Jensen J.O., Jorgensen H.E., 1970, A&A 5, 12
Däppen W., Mihalas D., Hummer D.G., Mihalas B.W., 1988, ApJ 332, 261
Fagotto F., Bressan A., Bertelli G., Chiosi C., 1994a, A&AS 104, 365
Fagotto F., Bressan A., Bertelli G., Chiosi C., 1994b, A&AS 105, 29
Girardi L., 1996, Ph.D. Thesis, Universidade Federal do Rio Grande do Sul, Porto Alegre, Brazil
Girardi L., 1999, MNRAS 308, 818
Girardi L., Bertelli G., 1998, MNRAS 300, 533
Girardi L., Bressan A., Chiosi C., Bertelli G., Nasi E., 1996a, A&AS 117, 113
Girardi L., Bressan A., Chiosi C., 1996b, in: Stellar Evolution: What Should Be Done, 32nd Liège Int. Astroph. Coll., Noels A., Frapont-Caro D., Gabriel M., Grevesse N., Demarque P. (eds.). Université de Liège, p. 39
Girardi L., Groenewegen M.A.T., Weiss A., Salaris M., 1998, MNRAS 301, 149
Graboske H.C., de Witt H.E., Grossman A.S., Cooper M.S., 1973, ApJ 181, 457
Grevesse N., Noels A., 1993, in: Origin and Evolution of the Elements, Pratzos N., Vangioni-Flam E., Cassé M. (eds.). Cambridge University Press
Groenewegen M.A.T., de Jong T., 1993, A&A 267, 410
Herwig F., 1996, in: Stellar Evolution: What Should Be Done, 32nd Liège Int. Astrophys. Coll., Noels A., Frapont-Caro D., Gabriel M., Grevesse N., Demarque P. (eds.). Université de Liège, p. 441
Høg E., Pagel B.E.J., Portinari L., et al., 1998, in: Primordial Nuclei and their Galactic Evolution, Prantzos N., Tosi M., von Steiger R. (eds.). ISSI, Bern. Kluwer: Dordrecht, Space Sci. Rev. 84, p. 115
Hubbard W.B., Lampe M., 1969, ApJS 18, 297
Hummer D.G., Mihalas D., 1988, ApJ 331, 794
Iben I., Truran J.W., 1978, ApJ 220, 980
Iglesias C.A., Rogers F.J., 1993, ApJ 412, 752
Itoh N., Kohyama, 1983, ApJ 275, 858
Itoh N., Mitake S., Iyetomi H., Ichimaru S., 1983, ApJ 273, 774
Jeffries R.D., 1997, MNRAS 288, 585
Kippenhahn R., Thomas H.-C., Weigert A., 1965, Z. Astrophys. 61, 241
Kurucz R.L., 1992, in: Stellar Populations of Galaxies, Barbuy B., Renzini A. (eds.). Dordrecht: Kluwer, p. 225
Landré V., Prantzos N., Aguer P., et al., 1990, A&A 240, 85
Maeder A., 1983, A&A 120, 113
Marigo P., 1998a, Ph.D. Thesis, University of Padua, Italy
Marigo P., 1998b, A&A 340, 463
Marigo P., Girardi L., Chiosi C., 1996, A&A 316, L1
Marigo P., Bressan A., Chiosi C., 1998, A&A 331, 564
Marigo P., Girardi L., Bressan A., 1999, A&A 344, 123
Meynet G., Maeder A., Schaller G., Schaerer D., Charbonnel C., 1994, A&AS 103, 97
Mihalas D., Däppen W., Hummer D.G., 1988, ApJ 331, 815
Mihalas D., Hummer D.G., Mihalas B.W., Däppen W., 1990, ApJ 350, 300
Munakata H., Kohyama Y., Itoh N., 1985, ApJ 296, 197
Pagel B.E.J., Portinari L., 1998, MNRAS 298, 747
Perryman M.A.C., Lindegren L., Kovalevsky J., et al., 1995, A&A 304, 69
Reimers D., 1975, Mem. Soc. R. Sci. Liege, Ser. 6, Vol. 8, p. 369
Renzini A., Fusi Pecci F., 1988, ARA&A 26, 199
Rogers F.J., Iglesias C.A., 1992, ApJS 79, 507
Straniero O., 1988, A&AS 76, 157
Vassiliadis E., Wood P.R., 1993, ApJ 413, 641
Weaver T.A., Woosley S.E., 1993, Phys. Rep. 227, 65
Weidemann V., 1987, A&A 188, 74
Weidemann V., 1996, in: Advances in Stellar Evolution, Rood R.T., Renzini A. (eds.). Cambridge University Press, p. 169